Time autocorrelation function analysis of master equation and its application to atomic clusters

Chi Zhang and R. Stephen Berry[a)]
Department of Chemistry, the University of Chicago, Chicago, Illinois 60637

(Received 14 April 2005; accepted 22 June 2005; published online 6 September 2005)

We derive the energy fluctuation $\Delta^2 E$, and the time autocorrelation $\kappa(\tau)$ and its Fourier transformation—the fluctuation spectra $S(\omega)$—of the master-equation transition matrix. The contribution from each eigenmode of the transition matrix to these fluctuation quantities reveals the relevant importance of the individual mode in the relaxation processes. The time scales associated with these relaxation processes are determined by the corresponding eigenvalues. Unlike traditional time evolution analysis, the autocorrelation function and fluctuation spectra analysis does not involve an arbitrary initial population. It is also more suitable for analyzing the underlying dynamic, kinetic behavior near the equilibrium and the behavior of the long-time-scale rare events. We utilize our technique to analyze the solid-liquid phase coexistence of the 13-atom Morse cluster and the fcc-to-icosahedral structure transition of the 38-atom Lennard-Jones cluster. For the processes studied, the fluctuation spectra from the master equation simplify the analysis of the transition matrix, and the important relaxation modes are easily extracted. © *2005 American Institute of Physics*. [DOI: 10.1063/1.2000243]

I. INTRODUCTION

The relaxation processes of complex chemical systems, such as clusters, glasses, peptides, and proteins, can exhibit a variety of different time evolution behaviors ranging from single exponential relaxation to multiexponential relaxation or asymptotic power-law relaxation.[1–5] These different relaxation behaviors are determined by the underlying potential-energy surfaces (PESs) of the systems if the temperature of the system is below the mode-coupling temperature, such that the local barriers between different wells on PES are larger than or comparable to the mean thermal kinetic energy of the system.

The time evolution of the physical properties can be described by stochastic master equation.[4–9] A natural way to define a state in the master equation is provided by the "inherent structure" analysis of the PES.[10] Except at high temperatures, the system will oscillate in the basin of attraction around a local minimum, and the sporadic jumping processes between the neighboring basins of attraction are Markovian. The region around a local minimum of the PES can be regarded as a state, and the saddle points on the PES determine the reaction rates of the jumping processes. The transition matrix can be built from the database of connected minima and saddle points, and the time evolution of the relaxation process can be solved after diagonalization of the transition matrix. The master equation generally takes less time to solve than molecular-dynamics (MD) simulation, since the only intensive calculations are the determination of minimum-to-minimum rate coefficients and the diagonalization of the transition matrix, and the average kinetic behavior is directly obtained. Previous studies of the master equation have generally concentrated on the time evolution analysis of probability flow from some specific initial population.[4,5,7,8] This is a straightforward approach to study the nonequilibrium relaxation process, but the effects of the arbitrary initial condition are yet to be resolved.

In this paper, we present our analysis of the time autocorrelation function and its fluctuation spectra derived from the master-equation transition matrix.[6] This approach is efficient at extracting the useful kinetics and dynamical information of complex systems near or approaching equilibrium without following the time evolution of some specific property or the knowledge of proper initial population. The time scale of the important relaxation kinetics and the corresponding dynamic mechanism can be studied systematically by inspecting the contribution of the transition matrix eigenmodes to the fluctuation properties and the respective fluctuation spectra from time autocorrelation function. The master equation and the time autocorrelation function derived from the transition matrix are discussed in Sec. II. The energy fluctuation spectra analysis of the time autocorrelation function is then applied to the phase coexistence of the 13-atom Morse cluster in Sec. III, and details of our analysis procedure are also presented. In Sec. IV we apply this approach to the structural transition kinetics analysis of the paradigmatic double-funnel PES 38-atom Lennard-Jones cluster. Finally, we summarize our conclusions of this contribution in Sec. V. In the following sections, all quantities are given in reduced units unless specified explicitly.

II. MASTER EQUATION

The master equation is a loss-gain equation that describes the time evolution of the probability $P_i(t)$ for finding the system in a state i. In our description of PES, every minimum on the PES corresponds to a unique state in the

[a)]Electronic mail: berry@uchicago.edu

 © 2005 American Institute of Physics

Downloaded 07 Sep 2005 to 128.135.233.79. Redistribution subject to AIP license or copyright, see http://jcp.aip.org/jcp/copyright.jsp

master equation, and the saddle points determine the state-to-state reaction rates. The basic form of the master equation is[6]

$$\frac{dP_i(t)}{dt} = \sum_j [k_{ij}P_j(t) - k_{ji}P_i(t)], \tag{1}$$

where k_{ij} is the transition rate from state j to state i, which in our study, is provided by the Rice-Ramsperger-Kassel-Marcus (RRKM) theory,[11]

$$k_{ij}(T) = \frac{kT}{h}\frac{Q_{ij}^{\ddagger}}{Q_j}\exp(-E_{ij}^{\ddagger}/kT), \tag{2}$$

where k is the Boltzmann constant, T the temperature, h the Planck constant, Q_j the partition function of the "reactant" state (or minimum) j, $Q_{ij}^{\ddagger}$ the partition function of the transition state linking states i and j, and $E_{ij}^{\ddagger}$ the energy barrier from state j to the transition state. Under the harmonic approximation, the partition function of minimum i at temperature T is

$$Q_i(T) = \frac{2N!}{h_i^{\mathrm{PG}}}\frac{(k_BT)^{\kappa}}{(h\prod_{i=1}^{\kappa}\nu_i)}e^{-V_i/k_BT}, \tag{3}$$

where N is the number of atoms, h_i^{PG} is the order of the point group of the isomer, ν_i is the ith vibrational frequency under harmonic assumption, $\kappa=3N-6$ is the number of vibrational freedom of a minimum, and for saddle point $\kappa=3N-7$; V is the potential energy of the stationary point.

A transition matrix $\mathbf{W}$ can be set up with the components

$$W_{ij} = k_{ij} - \delta_{ij}\sum_{m=1}^{n_{\min}} k_{mi}, \tag{4}$$

where $n_{\min}$ is the total number of minima, and the diagonal components W_{ii} contain minus the total rate constants from minimum i. The master equation can be rewritten in the matrix form as

$$\dot{\mathbf{P}}(t) = \mathbf{W}\mathbf{P}(t). \tag{5}$$

If $\mathbf{W}$ is not decomposable, then the system has one unique equilibrium state $\mathbf{P}^{\mathrm{eq}}$ for which $\dot{\mathbf{P}}|_{\mathbf{P}=\mathbf{P}^{\mathrm{eq}}}=0$, which means the matrix $\mathbf{W}$ has one single zero-value eigenvalue and its associated eigenvector corresponds to the equilibrium probability distribution. In general, $\mathbf{W}$ is asymmetric, but it can be transformed to a symmetric matrix under the detailed balance assumption

$$W_{ij}P_j^{\mathrm{eq}} = W_{ji}P_i^{\mathrm{eq}}. \tag{6}$$

The transformed symmetric matrix $\tilde{\mathbf{W}}$ where $\tilde{W}_{ij} = (P_j^{\mathrm{eq}}/P_i^{\mathrm{eq}})^{1/2}W_{ij}$ share the same eigenvalues as matrix $\mathbf{W}$, and their respective normalized eigenvectors $\tilde{\mu}^{(i)}$ and $\mu^{(i)}$ are related by $\mu^{(i)}=\mathbf{S}\tilde{\mu}^{(i)}$, where $\mathbf{S}$ is the diagonal transformation matrix $\mathbf{S}=\mathrm{diag}\{\sqrt{P_i^{\mathrm{eq}}}\}$. The analytic solution to the master equation is

$$P_i(t) = \sqrt{P_i^{\mathrm{eq}}}\sum_{j=1}^{n_{\min}}\tilde{\mu}_i^{(j)}e^{\lambda_j t}\left[\sum_{m=1}^{n_{\min}}\tilde{\mu}_m^{(j)}\frac{P_m(0)}{\sqrt{P_m^{\mathrm{eq}}}}\right], \tag{7}$$

or it may be written in a simpler matrix form,

$$\mathbf{P}(t) = \sum_{j=1}^{n} e^{\lambda_j t}(\mu\mu^T)^{(j)}\mathbf{P}'(0), \tag{8}$$

where $n=n_{\min}$ and $P_i'(t)=P_i(t)/P_i^{\mathrm{eq}}$.

Apart from the zero value, all other eigenvalues of the master equation λ_j are negative. If we label the eigenvalues in order of decreasing values, when $t\to\infty$, only the $\lambda_1=0$ terms survive, and $\mathbf{P}(t)\to\mathbf{P}^{\mathrm{eq}}$. The solution to the master equation suggests that the probability relaxation to the equilibrium shows a multiexponential behavior.

If one physical property A has a well-defined value in the master equation for each state i, the expectation value of A can be expressed as a weighted average as

$$\langle A(t)\rangle = \sum_{i=1}^{n} A_iP_i(t) = \sum_{i=1}^{n} A_i\sum_{j=1}^{n_{\min}}\mu_i^{(j)}e^{\lambda_j t}\left[\sum_{m=1}^{n_{\min}}\mu_m^{(j)}\frac{P_m(0)}{P_m^{\mathrm{eq}}}\right]. \tag{9}$$

If $\langle A\rangle_{\mathrm{eq}}=0$, the time autocorrelation function $\kappa(\tau)$ at equilibrium can be expressed as

$$\kappa(\tau) = \sum_{k=2}^{n} e^{\lambda_k\tau}\left[\sum_{i}^{n} A_i\mu_i^{(k)}\right]^2, \tag{10}$$

and the equilibrium fluctuation of A is

$$\langle A^2\rangle_{\mathrm{eq}} = \kappa(0) = \sum_{k=2}^{n}\left[\sum_{i=1}^{n} A_i\mu_i^{(k)}\right]^2. \tag{11}$$

Each eigenmode k of the transition matrix has a different contribution $\Sigma_{i=1}^{n}[A_i\mu_i^{(k)}]^2$ to the total fluctuation $\langle A^2\rangle$, and the eigenvalue $-\lambda_k$ corresponds to the jumping frequency of the fluctuation.

The Fourier transformation $S(\omega)$ of the time autocorrelation function $\kappa(\tau)$ is the fluctuation spectrum of A, and is given as

$$\begin{aligned} S(\omega) &= \frac{2}{\pi}\int_0^{\infty}\kappa(\tau)\cos(\omega\tau)d\tau \\ &= \frac{2}{\pi}\sum_{k=2}^{n}\frac{-\lambda_k}{\lambda_k^2+\omega^2}\left[\sum_{i=1}^{n} A_i\mu_i^{(k)}\right]^2. \end{aligned} \tag{12}$$

The form of the time correlation function κ shows how the individual components of the eigenvector $\mu_i^{(k)}$ contributes to the relaxation progress of A along the mode k. Or in the language of PES, a larger $|\mu_i^{(k)}|$ value suggests that the minimum i has a significant contribution to the relaxation mode k.

The low-frequency ($\omega\to 0$) and high-frequency ($\omega\to\infty$) limits of the fluctuation spectrum $S(\omega)$ exhibit how individual relaxation modes contribute to the overall long-time and short-time correlations, respectively,

$$S(\omega)|_{\omega\to\infty} = \sum_{k=2}^{n} S_k(\omega)|_{\omega\to\infty} = -\frac{2}{\pi\omega^2}\sum_{k=2}^{n}\lambda_k\left[\sum_{i=1}^{n} A_i\mu_i^{(k)}\right]^2, \tag{13}$$

Downloaded 07 Sep 2005 to 128.135.233.79. Redistribution subject to AIP license or copyright, see http://jcp.aip.org/jcp/copyright.jsp

$$S(\omega)|_{\omega\to 0} = \sum_{k=2}^{n} S_k(\omega)|_{\omega\to 0} = -\frac{2}{\pi}\sum_{k=1}^{n-1}\frac{1}{\lambda_k}\left[\sum_{i=1}^{n} A_i\mu_i^{(k)}\right]^2. \tag{14}$$

The contribution from individual modes, $\lambda_k[\Sigma_{i=1}^{n}A_i\mu_i^{(k)}]^2$ and $1/\lambda_k[\Sigma_{i=1}^{n}A_i\mu_i^{(k)}]^2$, gives us a picture of the relative importance of the mode k in the short-time and long-time fluctuations.

III. PHASE COEXISTENCE OF M_{13} CLUSTER

In this section, we use the fluctuation spectra of the the master-equation transition matrix to analyze the kinetics of phase coexistence behavior of the M_{13} cluster, the cluster of 13 atoms bounded by pairwise Morse potentials.

The Morse potential[12] is given by

$$V = \epsilon\sum_{i<j} e^{\rho(1-r_{ij}/\sigma)}[e^{\rho(1-r_{ij}/\sigma)} - 2]. \tag{15}$$

ϵ and σ are the dimmer potential well depth and equilibrium separation distance, respectively, and ρ is the dimensionless interaction range parameter. The interaction range between particles becomes longer as ρ decreases. Physically meaningful ρ values for diatomic molecules usually range from 3 to 7,[13,14] modeling the pairwise interactions from metals, which typically have longer force ranges, to noble gases, where the interactions are typically shorter ranged. Recently, the very short interaction between C_{60} molecules has been modeled with $\rho=13.6$.[15,16]

Small finite systems, such as atomic and molecular clusters, exhibit some of the solidlike and liquidlike behavior of bulk solids and liquids.[17–19] Under certain conditions, many clusters can coexist in well-defined solid- and liquid-phase-like forms. This coexistence, unlike the sharp coexistence curve of bulk solids and liquids, may exhibit itself over a finite band of temperature from T_f, below which the liquid has no stability, to T_m, above which the solid is no longer stable. For temperatures between T_f and T_m, the potential-energy distribution is bimodal. Previous studies have shown that such bimodality is greatly affected by the shape of the PES and its underlying interaction between particles.

Previous studies on the 13-atom clusters bounded by Morse potential (M_{13} cluster) have demonstrated that an increase of potential range can generally smooth the PES, eliminate the number of minima, make the solidlike structures easier to approach, and make the transition between the solid and liquid structures more frequent.[5,20,21] A quantitative description of the melting kinetics based on the master equation presented below can easily uncover the relationship between the kinetic and the dynamic behavior of the melting transition and its underlying PES topology.

The M_{13} PES database is constructed using the method proposed by Wales *et al.*[1] The number of minima and saddle points are listed in Table I. The database of $\rho=10$ and $\rho=14$ are provided by Miller *et al.*[20] Figure 1 shows the PES disconnectivity graphs of the M_{13} cluster with different range parameters. From the perspective based on the PES, at low temperatures below T_f, a cluster resides primarily in the low-energy minima with solidlike rigid structure(s), but as the temperature rises above T_f, the system populates those higher-energy minima with liquidlike structures, competitive with its population of the solidlike minima, until finally at melting temperature T_m, the minima with solidlike structure cannot compete with the liquid form and do not have significant dwell time. For the M_{13} cluster, the global minimum on the PES has a well-defined icosahedral geometry, with the solidlike properties under low temperatures.[20]

TABLE I. Number of minima and saddle points on the PES of the M_{13} cluster at different interaction ranges ρ.

ρ	4	6	10	14
Minima	162	1 466	9 306	12 760
Saddles	1 537	22 633	37 499	54 439

Figure 2 shows the equilibrium probability of the global minimum of the M_{13} cluster with different range parameters ρ. The curves show that decreasing the pairwise interaction range (increasing ρ) results in a lower freezing temperature, and a broadened coexistence range.

In the coexistence range from T_f through T_m, the heat capacity of the cluster has values larger than solid or liquid alone, which reflects the first-order phase-transition behavior. The heat-capacity change of the phase transition is associated with the configuration entropy change and the latent heat. We can define the configurational contribution to the heat capacity as

$$C_{vc} = \frac{\Delta E^2}{k_B T^2}, \tag{16}$$

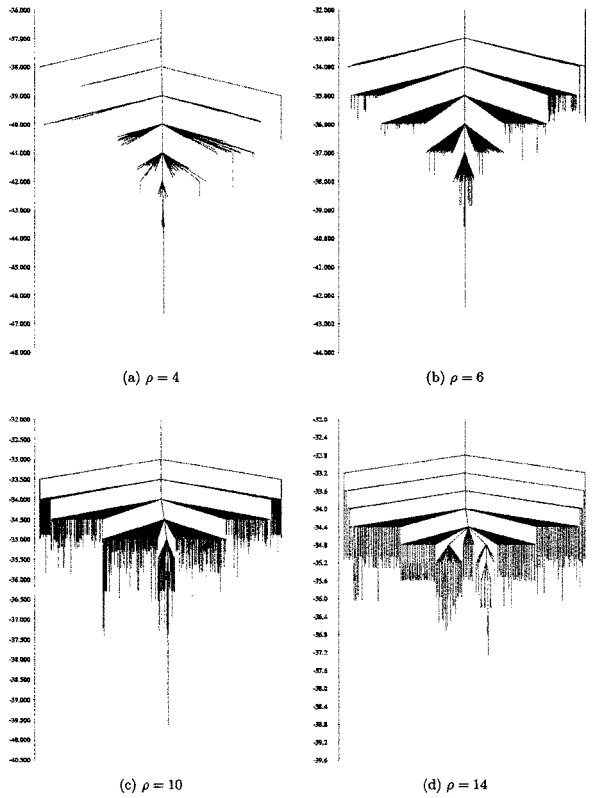

FIG. 1. PES disconnectivity graph of the M_{13} cluster. The vertical axis is the potential energy E in the unit of ϵ.

Downloaded 07 Sep 2005 to 128.135.233.79. Redistribution subject to AIP license or copyright, see http://jcp.aip.org/jcp/copyright.jsp

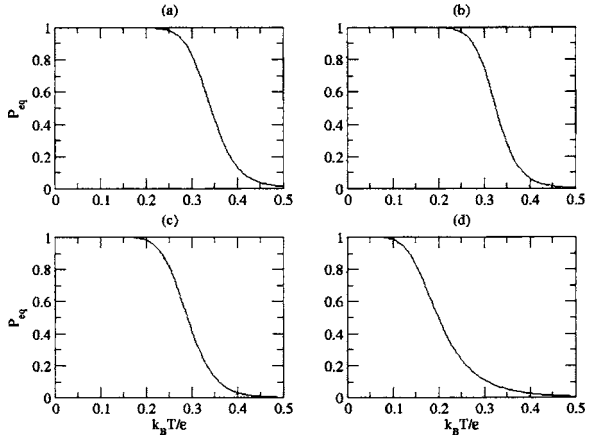

FIG. 2. Equilibrium probability of global minimum of the M_{13} cluster with different range parameters: (a) $\rho=4$, (b) $\rho=6$, (c) $\rho=10$, and (d) $\rho=14$. k_BT/ϵ and P_{eq} are the temperature in reduced units and equilibrium probability of global minimum, respectively.

$$\Delta E^2 = \sum_{i=1}^{n_{\min}} E_i^2 P_i^{\mathrm{eq}} - \left(\sum_{i=1}^{n_{\min}} E_i P_i^{\mathrm{eq}} \right)^2, \tag{17}$$

where ΔE^2 is the potential-energy fluctuation of the minima, T is the temperature, and E_i and P_i^{eq} are the potential-energy of minimum i and its corresponding equilibrium probability, respectively.

Figure 3 shows the configurational heat-capacity plots of the M_{13} cluster with different range parameter ρ. At $\rho=4$ and 6, the heat-capacity peaks are pronounced, which suggests a large latent heat associated with the phase transition. At $\rho=10$, the peak is broadened and the height is a bit smaller. The peak at $\rho=14$ is much lower but broader: the total area under the curve is much smaller, which implies that the latent heat is much smaller but the freezing limit T_f, the lower bound of the transition temperature region, is lowered to $T_f \sim 0.1$. It is interesting to note that the upper bounds of the peaks are almost the same, which indicates that the melting limit $T_m \sim 0.5$, and it does not depend on the range parameter ρ. When ρ is small, i.e., when the interaction range is long, the energy gap is large between the global minimum or other solidlike minima and other amorphous structured minima, which gives a larger latent heat and higher freezing temperature.

Four temperatures were examined within the melting temperature range between T_f and T_m by investigating the melting configuration heat-capacity curve so that those four values can represent the kinetic behavior from near T_f to near T_m. The potential-energy fluctuation ΔE^2, the long-time and

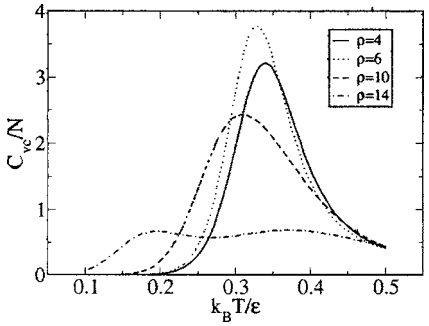

FIG. 3. Configurational heat capacity of the M_{13} cluster with different range parameters ρ. k_BT/ϵ and C_{vc}/N are the temperature and heat capacity per particle in reduced units, respectively.

short-time limits of the fluctuation spectra S_0 and S_∞ are investigated by using the master equation, as summarized in Table II. The total-energy fluctuation ΔE^2 has a pattern similar to the configurational heat capacity C_{vc}, which is what we expect from Eq. (16). S_∞ increases monotonically with temperature and interaction range (decreasing ρ), which reflects an overall fast kinetics with higher temperature and longer interaction range. The behavior of S_0 looks more irregular, which reflects the complexity of the overall PES topology as it has significant impact on the long-time kinetics.

More striking results are the fluctuation properties calculated from individual eigenmodes of the transition matrix to the kinetics, which are energy fluctuation $(\Delta E^2)_j$ and its short-time fluctuation spectra $S_\infty^{(j)}$ and long-time fluctuation spectra $S_0^{(j)}$, where j is the index of the eigenmodes; ∞ and 0 stand for the short-time limit $\omega \to \infty$ and long-time limit $\omega \to 0$, respectively, as denoted in Eqs. (13) and (14). Those quantities are calculated from

$$(\Delta E^2)_j = \sum_{i=1}^{n_{\min}} (E_i - \langle E \rangle)^2 [\mu_i^{(j)}]^2, \tag{18}$$

$$S_\infty^{(j)} = -\lambda_j (\Delta E^2)_j, \tag{19}$$

$$S_0^{(j)} = -\frac{1}{\lambda_j} (\delta E^2)_j, \tag{20}$$

where E_i is the potential-energy of minimum i, $\langle E \rangle$ is the average potential energy, $\mu_i^{(j)}$ is the ith component of the jth eigenvector, and λ_j is the corresponding eigenvalue. Equations (18)–(20) are the individual eigenmode components of Eqs. (11), (13), and (14). They reflect different contributions to the overall thermodynamics and kinetics from different

TABLE II. Eigenvalue characteristics of the transition matrix for the M_{13} cluster. T_1–T_4 are the temperatures chosen to diagonalize the transition matrix, where T_1 is near the freezing temperature T_f and T_4 is near the melting temperature T_m, ΔE_i^2 is the potential-energy fluctuation, and S_∞ and S_0 are the short- and long-time limits of the fluctuation spectra of the energy autocorrelation functions, as previously defined.

ρ	T_1	T_2	T_3	T_4	$\Delta E_{i,1}^2$	$\Delta E_{i,2}^2$	$\Delta E_{i,3}^2$	$\Delta E_{i,4}^2$	$S_{\infty,1}$	$S_{\infty,2}$	$S_{\infty,3}$	$S_{\infty,4}$	$S_{0,1}$	$S_{0,2}$	$S_{0,3}$	$S_{0,4}$
4	0.25	0.30	0.35	0.40	0.024	2.25	4.97	3.36	1.34	16.5	76.1	147	1.14	5.09	5.30	2.03
6	0.25	0.30	0.35	0.40	0.35	3.22	5.23	2.95	0.42	8.56	44.32	85.53	0.49	2.40	1.79	0.64
10	0.20	0.30	0.35	0.40	0.11	2.81	3.32	2.75	3.2×10^{-3}	1.78	6.77	13.00	21.25	18.12	4.55	1.46
14	0.10	0.20	0.30	0.40	7.6×10^{-3}	0.34	0.69	1.06	2.8×10^{-3}	9.2×10^{-2}	1.48	6.92	2.1×10^{-4}	31.29	1.08	0.82

Downloaded 07 Sep 2005 to 128.135.233.79. Redistribution subject to AIP license or copyright, see http://jcp.aip.org/jcp/copyright.jsp

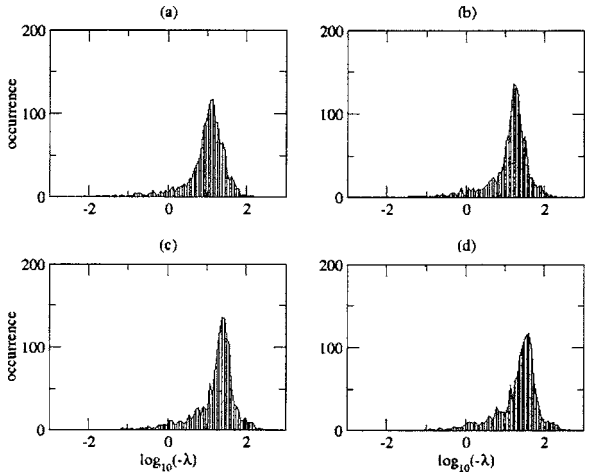

FIG. 4. Eigenvalue histogram of the transition matrix of the M_{13} cluster at $\rho=6$ at (a) $T=0.25$, (b) $T=0.30$, (c) $T=0.35$, and (d) $T=0.40$. T is the temperature and λ is the eigenvalue of the transition matrix; both are given in reduced units.

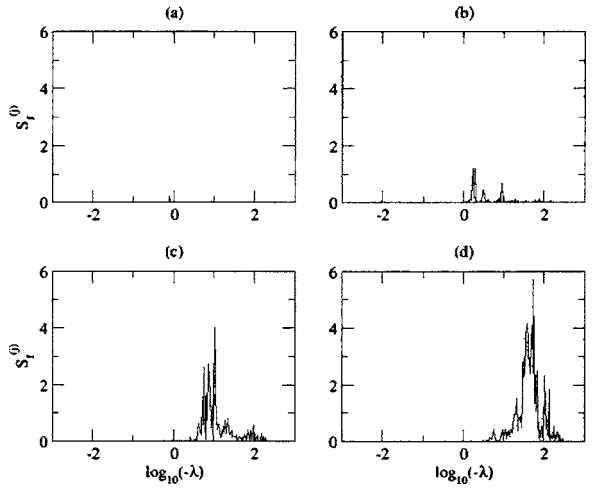

FIG. 6. $S_\infty^{(j)}$ plot of the M_{13} cluster with $\rho=6$ at (a) $T=0.25$, (b) $T=0.30$, (c) $T=0.35$, and (d) $T=0.40$.

eigenmodes and minima. The analysis of these quantities are presented below.

We first present our analysis of the M_{13} cluster with range parameter $\rho=6$. The overall histogram of the eigenvalues of the transition matrix contains little information about the kinetic behavior of the system as different eigenmodes have different importance, and these are not revealed in the plain equal-weight histogram. Figure 4 shows the eigenvalue histogram at $\rho=6$. The majority of the modes have the eigenvalues $\lambda \simeq 10^0 - 10^2$. The band of the eigenvalues shifts a bit to larger values as temperature increases, and the modes with smaller absolute eigenvalues shift faster than other modes. It is hard to tell how the individual modes affect the thermodynamic and kinetic quantities of the system.

Compared to the eigenvalue histogram, the plots of the energy fluctuation spectra $(\Delta E^2)_j$, the short-time limit of the fluctuation $S_\infty^{(j)}$, and the long-time limit $S_0^{(j)}$ have more information about the contribution of the individual modes to the energy fluctuation at different time scales. It is worthy to note that both S_∞ and S_0 plots are relatively robust to the PES database, although a few higher-energy dead-end minima may introduce noisy lines in the S_0 plots, which are easily detected, and those minima are trimmed off from the PES database, as described in the literature.[5,20]

Figures 5–7 are the plots of $(\Delta E^2)_j$, $S_\infty^{(j)}$, and $S_0^{(j)}$ of M_{13} at $\rho=6$, respectively. The eigenmodes are highly filtered in these plots. At the low temperature $T=0.25$, all three plots have a common peak around $-\lambda \simeq 1$, and the typical relaxation time is around $\tau \simeq 1$ in reduced time units, or the order of 10^{-12} s if we use the physical constants of argon atoms. This relaxation time is much slower than the typical vibration periods of argon clusters, which are around $10^{-14}-10^{-13}$ s, the same order as most of the relaxation modes of the transition matrix. At the onset of the phase coexistence $T=0.25$, these modes are the only modes that have significant contribution to the energy fluctuation and its short-time and long-time spectra, which implies that the kinetics and underlying dynamics are relatively simple at this temperature. As the temperature rises to $T=0.30$, this peak shifts to larger $-\lambda$ values, the relaxation gets faster, and the three plots of $(\Delta E^2)_j$, $S_\infty^{(j)}$, and $S_0^{(j)}$ show different patterns. This peak eventually disappears as temperature grows even higher; the energy fluctuation $(\Delta E^2)_j$ is smaller, as expected

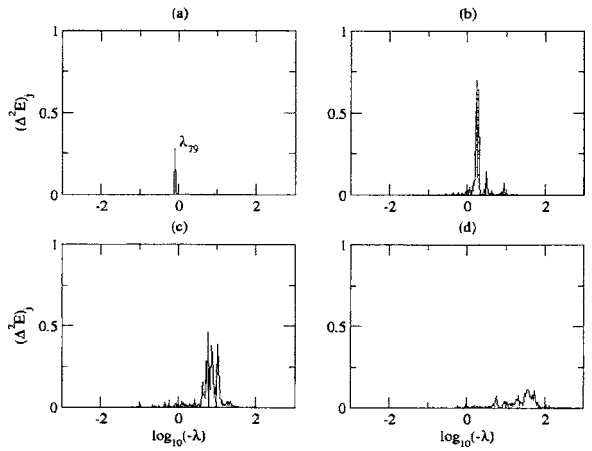

FIG. 5. $(\Delta E^2)_j$ plot of the M_{13} cluster with $\rho=6$ at (a) $T=0.25$, (b) $T=0.30$, (c) $T=0.35$, and (d) $T=0.40$.

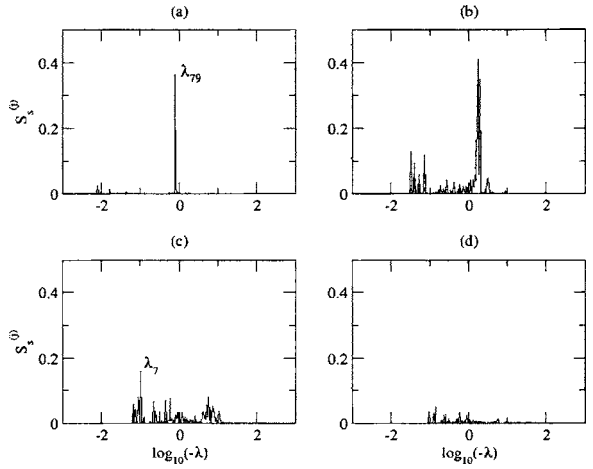

FIG. 7. $S_0^{(j)}$ plot of the M_{13} cluster with $\rho=6$ at (a) $T=0.25$, (b) $T=0.30$, (c) $T=0.35$, and (d) $T=0.40$.

Downloaded 07 Sep 2005 to 128.135.233.79. Redistribution subject to AIP license or copyright, see http://jcp.aip.org/jcp/copyright.jsp

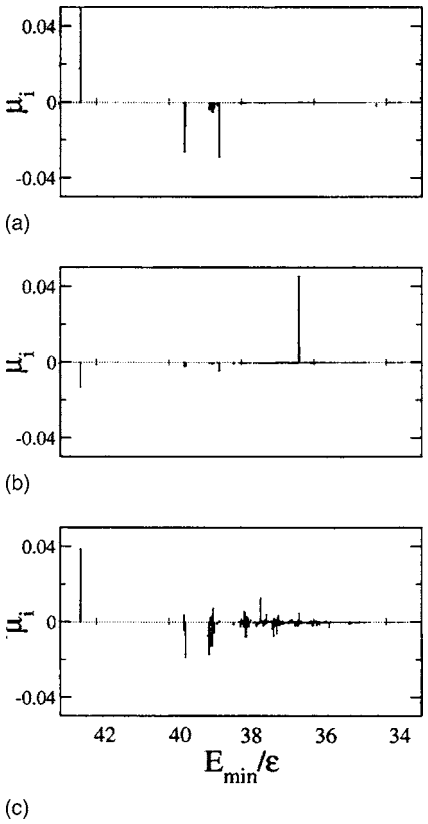

FIG. 8. Eigenvector plots of M_{13} with $\rho=6$: (a) $T=0.25$, $\lambda_{79}=-0.77$; (b) $T=0.35$, $\lambda_7=-0.10$; and (c) $T=0.40$, $\lambda_{1240}=-56.3$.

from the total heat-capacity change. The long-time limit of the energy fluctuation spectra $S_0^{(j)}$ has some modes slower than the major peak at $T=0.30$, but those modes do not make significant contribution at higher temperatures, and the total value of S_0 is smaller too, meaning that the long-time behavior is not as prominent as at low temperatures. The short-time limit of the fluctuation spectra $S_\infty^{(j)}$ shows a different pattern: The heights of peaks are fairly small at low temperatures $T=0.25-0.30$, at similar positions as the energy fluctuation plot $(\Delta E^2)_j$ at higher temperatures $T=0.35-0.40$, $S_\infty^{(j)}$ has unique features with much larger and broader peaks on the right side of the plots, at the same position as the peak of the nonweighted plain histogram of eigenvalues, which means that at higher temperatures where the system is more liquidlike, the most significant relaxation modes are more like the typical vibrational motions, which has the same time scales as those modes.

More detailed information of the important relaxation modes can be obtained by analysis of the corresponding eigenvectors, as shown in Fig. 8.

Figure 8(a) shows the eigenvector components of the mode $\lambda_{79}=-0.77$ at $T=0.25$. This mode has the largest contributions to all the fluctuation quantities $(\Delta E^2)_j$, $S_\infty^{(j)}$, and $S_0^{(j)}$. This mode corresponds to the probability flow between the global icosahedral minimum (peak 1) and other minima with one or two atoms out of the icosahedral outer shell (peaks 2 and 3), which is the prominent kinetic motion at the low-temperature limit of the phase coexistence region. Figure 8(b) shows the components of the eigenvector associated

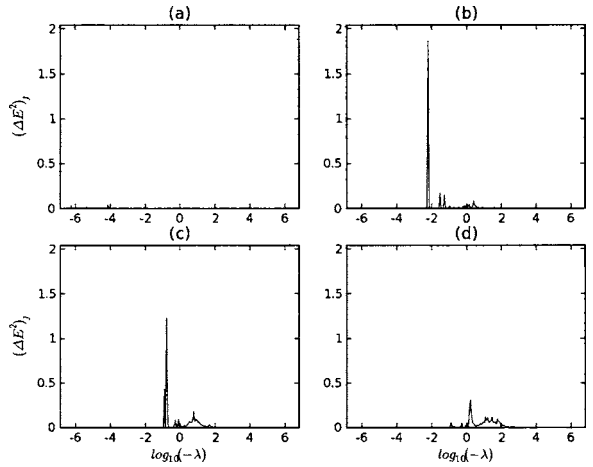

FIG. 9. $(\Delta E^2)_j$ plot of the M_{13} cluster with $\rho=10$ at (a) $T=0.20$, (b) $T=0.30$, (c) $T=0.35$, and (d) $T=0.40$.

with the peak pointed out in Fig. 7(c), which has the eigenvalue of $\lambda_7=-0.10$ at $T=0.35$. This is one of the slowest modes, with probability flows between the global minimum and a higher-energy minimum. This mode is more like a minimum-to-minimum transition, and the only connectivity of the higher-energy minimum is the global minimum, linked with a high-energy barrier. Figure 8(c) is the eigenvector plot of the relaxation mode $\lambda_{1240}=-56.3$. This mode only appears at higher temperatures of the phase coexistence region; it has a larger number of minima involved, especially those corresponding to liquid structures.

The fluctuation spectra of the M_{13} cluster at other ρ values are also investigated. The fluctuation spectra of $\rho=4$ looks similar to the spectra of $\rho=6$, but the relaxation modes with larger fluctuation values have larger eigenvalues than their $\rho=6$ counterparts, which reflects the fact that the relaxation processes of $\rho=4$ are faster than $\rho=6$. The relaxations of the $\rho=10$ cluster is even slower. Figures 9–11 show the fluctuation spectra of $\Delta^2 E^{(j)}$, $S_\infty^{(j)}$, and $S_0^{(j)}$ at $\rho=10$. The largest peaks in Figs. 9 and 11 correspond to the transition modes of solid to low-energy liquid structures, with large energy fluctuations. The short-time limit of the energy fluctuation spectra $S_\infty^{(j)}$ at $\rho=10$ (Fig. 10) has a much broader

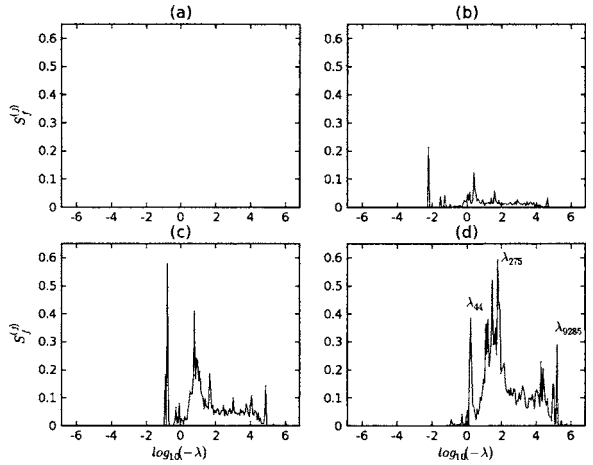

FIG. 10. $S_\infty^{(j)}$ plot of the M_{13} cluster with $\rho=10$ at (a) $T=0.20$, (b) $T=0.30$, (c) $T=0.35$, and (d) $T=0.40$.

Downloaded 07 Sep 2005 to 128.135.233.79. Redistribution subject to AIP license or copyright, see http://jcp.aip.org/jcp/copyright.jsp

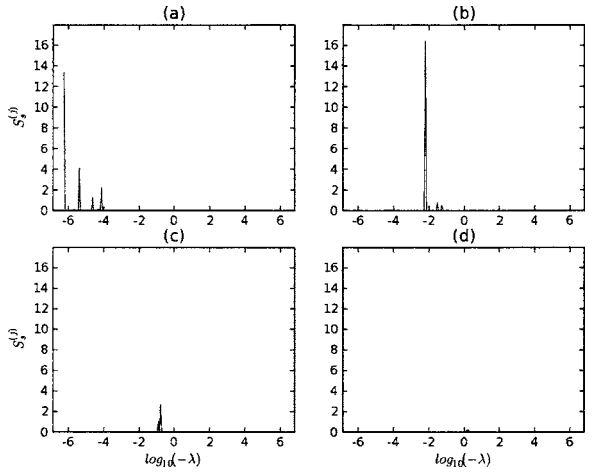

FIG. 11. $S_0^{(j)}$ plot of the M_{13} cluster with $\rho=10$ at (a) $T=0.20$, (b) $T=0.30$, (c) $T=0.35$, and (d) $T=0.40$.

range than $\rho=4$ and $\rho=6$. The multipeak feature of the $S_\infty^{(j)}$ plots reflects the multiplicity of short-time-scale relaxation processes and the complexity of the underlying PES. Figure 12 shows the eigenvector components of the three relaxation modes λ_{44}, λ_{275}, and λ_{9285} of Fig. 10(d). Mode λ_{44} corresponds to the jumping processes between the lower-lying energy minima and some isolated high-energy minima. Mode λ_{275} has a large number of minima involved with multistep processes. Relaxation mode λ_{9285} represents the probability flow mainly between the minimum $E=-36.67\epsilon$ and minimum $E=-35.17\epsilon$. The results of $\rho=14$ follows a similar

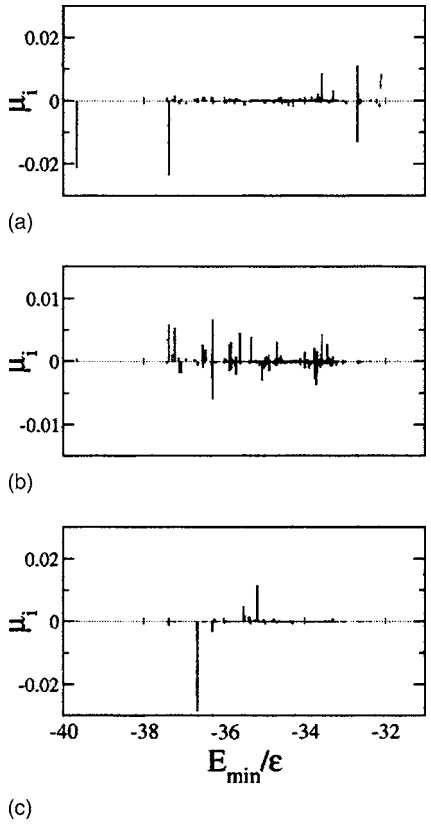

FIG. 12. Plots of eigenvector components μ of the M_{13} cluster at $\rho=10$, $T=0.40$: (a) μ plot with eigenvalue $\lambda_{44}=-1.251$, (b) μ plot with eigenvalue $\lambda_{275}=-3.161$ (c), and μ plot with eigenvalue $\lambda_{9285}=-185.5$.

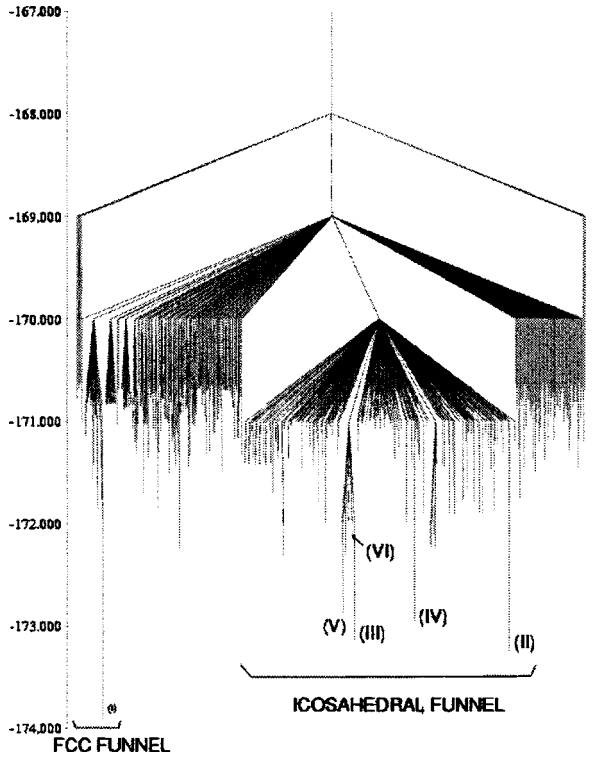

FIG. 13. Disconnectivity graph of the LJ_{38} cluster. Only the lowest 5000 minima are shown in the graph. The vertical axis is the potential energy in the unit of ϵ.

pattern as $\rho=10$, but the fluctuation values are smaller due to the fact the the total configurational energy fluctuation with $\rho=14$ is smaller and the phase transition at $\rho=14$ is not so obvious.

IV. STRUCTURE TRANSITION OF LJ_{38} CLUSTER

The Lennard-Jones potential[22] is given by

$$V=\sum_{i<j} 4\epsilon\left[\left(\frac{\sigma}{r}\right)^{12}-\left(\frac{\sigma}{r}\right)^{6}\right], \tag{21}$$

where σ is the separation of distance of dimer at zero potential energy, and ϵ is the well depth of the dimer.

The 38-atom Lennard-Jones cluster (LJ_{38}) has a double-funnel potential-energy landscape.[5,23,24] The PES disconnectivity graph of LJ_{38} is shown in Fig. 13. It is practically impossible to sample the full PES of the LJ_{38} cluster as the number of stationary points on the PES is too large. Here we primarily concentrated on the energetically low-lying region of PES associated with the two funnels. Our database of LJ_{38} consists of the 6000 minima with the lowest potential energy and the 8633 saddle points connecting those minima.[5] The global minimum of the PES lies at the bottom of the narrower funnel with fcc packing, but there is another funnel with higher energy, much larger volume in configuration space, and icosahedrally packed geometry. The relaxation from liquidlike structures to the global minimum of the PES will be trapped by the icosahedral funnel because its volume is larger and its structures are more similar to those of the liquid. The high barrier between the two states makes the transition between the two structures a slow process, beyond

Downloaded 07 Sep 2005 to 128.135.233.79. Redistribution subject to AIP license or copyright, see http://jcp.aip.org/jcp/copyright.jsp

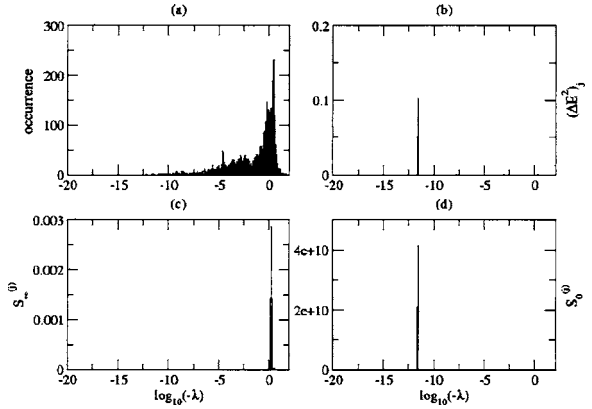

FIG. 14. Eigenvalue spectra of the transition matrix for the LJ_{38} cluster at $T=0.1$: (a) non-weighted histogram, (b) energy fluctuation $(\Delta E^2)_j$, (c) short-time limit of energy fluctuation spectrum $S_\infty^{(j)}$, and (d) long-time limit of energy fluctuation spectrum $S_0^{(j)}$.

the typical simulation time scale of molecular dynamics. The competition between the fcc funnel with lower energy but smaller configuration entropy and the icosahedral bowl with larger entropy but higher energy leads to a structural transition occurring around $T\sim 0.1$ under the harmonic superposition approximation, above which the icosahedral structure has a lower free energy than the fcc structure.[5] Master-equation analysis is a proper tool to study the slow transition. It is possible to analyze the eigenvector components of all the slow relaxation modes, calculate the probability flow of the modes, and get the relaxation mode(s) corresponding to the probability flow between the two funnels. With the aid of the fluctuation quantities we developed, it is much easier to find the mode, as presented below.

Figure 14 shows the eigenvalue spectrum analysis plots of the LJ_{38} transition matrix at $T=0.1$. The nonweighted histogram spans the range $-\lambda \simeq 10^{-13}-10^{2}$, and the peak occurrence value is around $-\lambda \geqslant 1$. The largest peak in the plots of $(\Delta E^2)_j$ and $S_0^{(j)}$ [Figs. 14(b) and 14(d)], with the eigenvalue of $\lambda_4=-2.5\times 10^{-12}$, is the relaxation mode of the fcc to icosahedron structure transition. If we use the physical constants of argon atoms, the relaxation time of this mode is ~ 0.8 s, which is much longer than the capacity of current MD simulations. The eigenvector components of this relaxation mode are shown in Fig. 15(a). Peak 1 in plot (a) is the global energy minimum [minimum (i) in Fig. 13] in the fcc funnel and the peaks in group 2 [minimum (ii) in Fig. 13] are the lowest-energy minima in the icosahedral funnel; the opposite signs of the two groups indicate that the probability flows of the two funnels have opposite directions. This mode has been discussed in detail in the literature,[5] and here we present a more straightforward approach to locate it.

Besides the prominent interfunnel transition mode discussed above, there are other important intrafunnel modes which can be detected from the fluctuation spectra analysis.

Although there are many fast relaxation modes shown in the nonweighted histogram, there is only one prominent peak in the plot of the short-time limit of the fluctuation spectrum $S_0^{(j)}$ with the eigenvalue $\lambda_{4548}=-1.71$; this mode is actually the jumping mode between two local minima, (iii) and (vi) in Fig. 13, of the icosahedral funnel. The eigenvector components of this relaxation mode are presented in Fig. 15(b). The two main peaks in plot (b) correspond to two connected minima in the icosahedral funnel; they have opposite directions of probability flow, as expected. The energies of the two minima are $E_1=-172.235\epsilon$ [minimum (iii)] and $E_2=-173.131\epsilon$ [minimum (vi)], and the saddle point between the two minima has a low energy of $E_s=-172.238\epsilon$, making it a fast transition mode. It may be hard to distinguish the two minima even at a temperature as low as $T=0.10$.

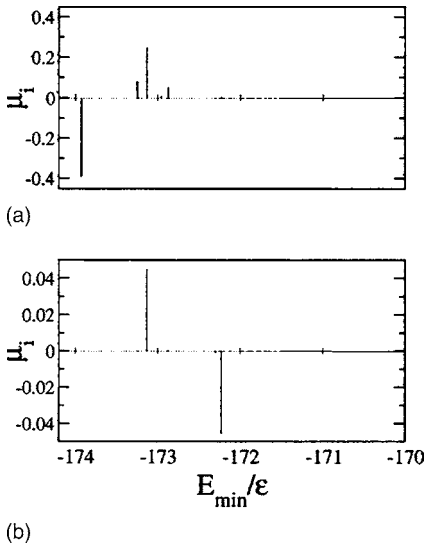

FIG. 15. Important eigenvectors of the LJ_{38} transition matrix. (a) fcc to icosahedral transition mode $\lambda_4=-2.5\times 10^{-12}$: (1) the global minimum in the fcc funnel and (2) the lowest-energy minima in the icosahedral funnel. (b) Fast mode in the icosahedral funnel $\lambda_{4548}=-1.71$.

Careful examination of the energy fluctuation plot (ΔE^2) (Fig. 16) recovers a few intrafunnel transition modes. Modes λ_4 and λ_{4548} have been discussed above. Mode λ_{97} is the transition mode between minima (ii) and (iii), the two minima with the lowest energy in the icosahedral funnel in Fig. 13. The relaxation process between the two is relatively slow compared to most other modes ($\lambda_{97}=-1.44\times 10^{-8}$), as the two minima are not directly connected and the relaxation may involve a set of high-energy saddle points and minima. Mode $\lambda_{183}=-4.08\times 10^{-7}$ is the relaxation mode between minima (ii) and (iv); and mode $\lambda_{1158}=-7.11\times 10^{-4}$ is the relaxation mode between minima (iii) and (iv). All the modes discovered and the transitions between the lowest-lying minima are inside the icosahedral funnel.

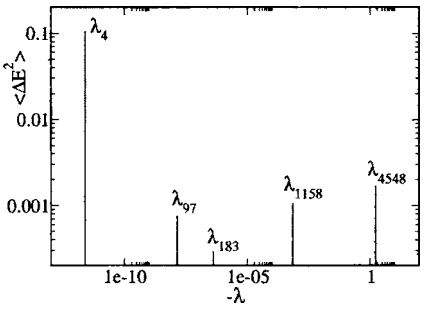

FIG. 16. Logscale plot of energy fluctuation $(\Delta E^2)_j$ of the LJ_{38} cluster at $T=0.1$.

Downloaded 07 Sep 2005 to 128.135.233.79. Redistribution subject to AIP license or copyright, see http://jcp.aip.org/jcp/copyright.jsp

V. CONCLUSION

To conclude, a new approach to master-equation analysis based on fluctuation spectra and time autocorrelation functions is presented. This method does not require the knowledge of an initial probability population, and kinetic behavior toward or near the equilibrium can be easily interpreted or predicted.

The fluctuation spectra approach filters the eigenvalue spectra of the transition matrix such that the relevant important eigenmodes to the fluctuation can be identified and characterized. The relaxation time of this fluctuation is directly related to the eigenvalue of the important eigenmodes. The relationship between the relaxation process and its underlying PES can be discovered by analysis of the corresponding eigenvectors.

Fluctuation spectra analysis of the solid-liquid coexistence of the M_{13} cluster shows that at the low-temperature limit of the solid-liquid coexistence region, only a few relaxation modes associated with solidlike structure and surface-defected structural transition are observable, but as the temperature rises, the short-time and the long-time behavior of the fluctuations diverge. There are some long-time relaxation modes corresponding to the jumping motion between solidlike structures and some higher-energy surface-defected or amorphous structures, but the short-time relaxation processes dominate at higher temperatures and long-time fluctuations are depressed. Transitions between the fcc and icosahedral structures of LJ_{38} has been a paradigmatic example of a slow kinetic process on a complex PES. The fluctuation spectra analysis at $T=0.10$ can pick this mode directly without exhaustive examination of the individual modes.

ACKNOWLEDGMENTS

We thank Dr. David J. Wales and Dr. Mark Miller for providing their PES database of the M_{13} cluster with $\rho=10,14$ and the LJ_{38} cluster. One of the authors (C.Z.) thanks Dr. Arthur Reber and Jun Lu for helpful discussions. This research is supported by NSF.

APPENDIX: TIME AUTOCORRELATION FUNCTION IN MASTER EQUATION

We begin with the solution to the master equation:

$$P_i(t)=\sum_{j=1}^{n_{\min}}\mu_i^{(j)}e^{\lambda_j t}\left[\sum_{m=1}^{n_{\min}}\mu_m^{(j)}\frac{P_m(0)}{P_m^{\mathrm{eq}}}\right]. \tag{A1}$$

We assume that the physical property we study is A which has a well-defined value A_i in each state i of a system with totally n discrete states, where $\langle A\rangle_{\mathrm{eq}}=0$, and the time relaxation of A near equilibrium can be described by the master equation. The probability of observing state i at time t is $P_i(t)$, so $P(i,0;j,t)$, which is our probability of observing the system at state i at time 0 and observing state j at time t, respectively, is

$$P(i,0;j,t)=P_i(0)\sum_{k=1}^{n}e^{\lambda_k t}\mu_j^{(k)}\frac{\mu_i^{(k)}}{P_i^{\mathrm{eq}}}, \tag{A2}$$

where $n=n_{\min}$ is the total number of minima on the PES.

Therefore the time autocorrelation of A at equilibrium, where $P_i(0)=P_i^{\mathrm{eq}}$, is

$$\begin{aligned}\kappa(\tau)=\langle A(0)A(t)\rangle&=\sum_{i,j}^{n}A_iA_jP(i,0;j,t)\\&=\sum_{i,j}^{n}A_iA_jP_i(0)\sum_{k=1}^{n}e^{\lambda_k t}\mu_j^{(k)}\frac{\mu_i^{(k)}}{P_i^{\mathrm{eq}}}\\&=\sum_{k=1}^{n}e^{\lambda_k t}\sum_{i}^{n}A_i\mu_i^{(k)}\sum_{j}^{n}A_j\mu_j^{(k)}=\sum_{k=1}^{n}e^{\lambda_k t}\left[\sum_{i}^{n}A_i\mu_i^{(k)}\right]^2\\&=\sum_{k=2}^{n}e^{\lambda_k t}\left[\sum_{i}^{n}A_i\mu_i^{(k)}\right]^2\qquad\left(\sum_{i}^{n}A_i\mu_i^{(n)}=\langle A\rangle_{\mathrm{eq}}=0\right).\end{aligned}$$

The fluctuation of A is given by

$$\begin{aligned}\langle A^2\rangle=\kappa(0)&=\sum_{k=1}^{n}\left[\sum_{i=1}^{n}A_i\mu_i^{(k)}\right]^2\\&=\sum_{k=1}^{n}\left\{\sum_{i=1}^{n}A_i^2[\mu_i^{(k)}]^2+\sum_{i<j}^{n}A_iA_j\mu_i^{(k)}\mu_j^{(k)}\right\}\\&=\sum_{i,k}^{n}A_i^2[\mu_i^{(k)}]^2+\sum_{i<j}^{n}A_iA_j\sum_{k=1}^{n}\mu_i^{(k)}\mu_j^{(k)}\\&=\sum_{i,k}^{n}A_i^2[\mu_i^{(k)}]^2+\sum_{i<j}^{n}A_iA_j\sqrt{P_i^{\mathrm{eq}}P_j^{\mathrm{eq}}}\sum_{k=1}^{n}\tilde{\mu}_i^{(k)}\tilde{\mu}_j^{(k)}\\&=\sum_{i,k}^{n}A_i^2[\mu_i^{(k)}]^2+\sum_{i<j}^{n}A_iA_j\sqrt{P_i^{\mathrm{eq}}P_j^{\mathrm{eq}}}\delta(i,j),\end{aligned}$$

where $\delta(i,j)=0$ when $i\neq j$ and $\delta(i,i)=1$. We have

$$\langle A^2\rangle=\sum_{k=1}^{n}\sum_{i=1}^{n}A_i^2[\mu_i^{(k)}]^2. \tag{A3}$$

On the other hand, the fluctuation of A can also be written as

$$\langle A^2\rangle=\sum_{i=1}^{n}A_i^2P_i^{\mathrm{eq}}. \tag{A4}$$

Hence we have the relation between Eqs. (A3) and (A4):

$$P_i^{\mathrm{eq}}=\sum_{k=1}^{n}[\mu_i^{(k)}]^2. \tag{A5}$$

Equation (A5) can also be derived from the normalization of the eigenvectors $\tilde{\mu}$.

[1] D. J. Wales, J. P. K. Doye, M. A. Miller, P. N. Mortenson, and T. R. Walsh, Adv. Chem. Phys. **115**, 1 (2000).
[2] M. Gruebele, Annu. Rev. Phys. Chem. **50**, 485 (1999).
[3] J. J. R. Metzlera, J. Klafter, and M. Volk, Chem. Phys. Lett. **293**, 477 (1998).

Downloaded 07 Sep 2005 to 128.135.233.79. Redistribution subject to AIP license or copyright, see http://jcp.aip.org/jcp/copyright.jsp

[4] Y. Levy, J. Jortner, and R. S. Berry, Phys. Chem. Chem. Phys. **4**, 5052 (2002).
[5] M. A. Miller, J. P. K. Doye, and D. J. Wales, Phys. Rev. E **60**, 3701 (1999).
[6] N. G. van Kampen, *Stochastic Processes in Physics and Chemistry* (North-Holland, Amsterdam, 1981).
[7] K. D. Ball and R. S. Berry, J. Chem. Phys. **109**, 8541 (1998).
[8] K. D. Ball and R. S. Berry, J. Chem. Phys. **109**, 8557 (1998).
[9] R. E. Kunz, P. Blaudeck, K. H. Hoffmann, and R. S. Berry, J. Chem. Phys. **108**, 2576 (1998).
[10] F. Stillinger and T. Weber, Phys. Rev. A **25**, 978 (1982).
[11] R. G. Gilbert and S. C. Smith, *Theory of Unimolecular and Recombination Reactions* (Blackwell, Oxford, 1990).
[12] P. M. Morse, Phys. Rev. **34**, 57 (1929).
[13] L. A. Girifalco and V. G. Weizer, Phys. Rev. **114**, 687 (1959).
[14] L. A. Girifalco, J. Phys. Chem. **96**, 858 (1992).
[15] J. Doye and D. J. Wales, J. Chem. Soc., Faraday Trans. **90**, 1061 (1994).
[16] D. J. Wales and J. Uppenbrink, Phys. Rev. B **50**, 12342 (1994).
[17] R. S. Berry, Microscale Thermophys. Eng. **1**, 1 (1997).
[18] J. Jellinek, T. L. Beck, and R. S. Berry, J. Chem. Phys. **84**, 2783 (1986).
[19] H. L. Davis, J. Jellinek, and R. S. Berry, J. Chem. Phys. **86**, 6456 (1987).
[20] M. A. Miller, J. P. K. Doye, and D. J. Wales, J. Chem. Phys. **110**, 328 (1999).
[21] M. Moseler and J. Nordiek, Phys. Rev. B **60**, 11734 (1999).
[22] J. E. Jones and A. E. Ingham, Proc. R. Soc. London, Ser. A **107**, 636 (1925).
[23] J. P. Doye, M. A. Miller, and D. J. Wales, J. Chem. Phys. **111**, 8417 (1999).
[24] J. P. K. Doye, M. A. Miller, and D. J. Wales, J. Chem. Phys. **110**, 6896 (1999).

Downloaded 07 Sep 2005 to 128.135.233.79. Redistribution subject to AIP license or copyright, see http://jcp.aip.org/jcp/copyright.jsp